npj | digital medicine

Article

Published in partnership with Seoul National University Bundang Hospital

https://doi.org/10.1038/s41746-025-02239-0

A novel single-cell level evaluation method for corneal endothelial cell function

Dongfang Li[1,2,3,8], Zongyi Li[1,2,3,8], Haoyun Duan[1,2,3], Xinhang Wang[4], Zhan Lin[5], Kun Dai[4], Quan Qi[6], Yanling Dong[1,2], Ping Lin[1,2], Wenjie Su[1,2], Shuting Wang[7], Xiangyue Hu[1,2], Xiaojing Pan[1,2], Xiaomin Liu[1,2], Qingjun Zhou[1,2,3] ✉ & Lixin Xie[1,2,3] ✉

Approximately 10 million people worldwide suffer from corneal diseases, with endothelial dysfunction being a leading cause of blindness. Current morphological assessments lack sensitivity for detecting early corneal endothelial abnormalities. Here, we present a novel diagnostic framework that evaluates endothelial cell function at the single-cell level by analyzing morphological alterations. Using machine learning, we developed an image-based recognition system to digitize cellular features. By applying geometric and mathematical principles, we established the "Xin-Value" (XV) as a new functional metric. In several corneal endothelial injury models, XV strongly correlated with mitochondrial function and stress markers, confirming its biological relevance. Leveraging XV, we refined a grading system for endothelial damage, demonstrating improved accuracy across clinicians of varying expertise. This study introduces a paradigm shift in corneal endothelial assessment, enabling highly sensitive, image-based detection of early dysfunction at the single-cell level, with potential applications in clinical screening and disease monitoring.

Corneal endothelial cells (CECs) form a monolayer of hexagonal cells lining the inner surface of the cornea, functioning as a pump-barrier to regulate stromal hydration and maintain optical clarity[1]. In humans, CECs exhibit limited proliferative capacity in vivo. Following injury, repair primarily occurs through migration and enlargement of adjacent endothelial cells[2]. Endothelial cell density (ECD) naturally decreases with age at an average rate of approximately 0.6% per year[3]. When ECD falls below 400–700 cells/mm², decompensation may ensue, leading to corneal edema, loss of transparency, and potentially blindness[4]. Globally, an estimated 12.7 million individuals suffer from corneal blindness, with mounting evidence implicating corneal endothelial dysfunction as a leading etiological factor[5,6].

Clinical diagnosis of corneal endothelial disease relies on imaging modalities including specular endothelial microscopy, pachymetry, confocal microscopy, and slit-lamp biomicroscopy. Central analysis of specular endothelial microscopy, recognized by the U.S. FDA as the gold standard, is widely adopted for evaluating corneal endothelial dysfunction[7,8]. Although manual analysis provides high accuracy—requiring technicians to delineate regions and mark cell centers—it is labor-intensive, time-consuming, and prone to subjectivity. Subsequent software processing quantifies key morphological parameters such as ECD, coefficient of variation in cell area (CV), and hexagonality (HEX). Over the past decades, artificial intelligence (AI)—particularly deep learning—has been increasingly applied in ophthalmology, demonstrating high performance in detecting corneal, retinal, and optic nerve pathologies, significantly improving corneal endothelial image segmentation and feature recognition[9–13]. However, current technologies remain limited in their ability to assess CEC function, highlighting an unmet clinical need.

Clinical imaging provides essential information on CEC morphology and density, with ECD serving as a key clinical indicator of corneal endothelium. Functional decompensation typically occurs when ECD falls below 400–700 cells/mm², though long-term studies show that corneal clarity and thickness can remain stable even at these low densities, particularly in post-penetrating keratoplasty (PK) patients followed for over a decade[14–16]. CECs form a tightly packed monolayer, predominantly hexagonal in shape—a configuration favored by the principle of minimal interfacial energy[17]. While hexagonal cells constitute 48–90% of the population, pentagonal (15–35%) and heptagonal (25–38%) cells are also common[18–20]. Corneal endothelial pathology is marked by reduced ECD and increased pleomorphism and polymegethism, leading to vision impairment[21]. Current morphometric analyses focus on overall HEX and CV; however, these metrics lack

[1]Eye Institute of Shandong First Medical University, Qingdao Eye Hospital of Shandong First Medical University, Qingdao, China. [2]School of Ophthalmology, Shandong First Medical University, Jinan, China. [3]State Key Laboratory Cultivation Base, Shandong Key Laboratory of Eye Diseases, Qingdao, China. [4]QingDao CEPC CAE Technology Co., Ltd, Qingdao, China. [5]School of Public Health, Tianjin Medical University, Tianjin, China. [6]School of Computer Science and Technology, Shihezi University, Shihezi, China. [7]Eye Institute of Shandong First Medical University, Eye Hospital of Shandong First Medical University (Shandong Eye Hospital), Jinan, China. [8]These authors contributed equally: Dongfang Li, Zongyi Li. ✉e-mail: qjzhou2000@126.com; lixin_xie@hotmail.com

sensitivity to single-cell shape dynamics and do not reflect individual cell function.

Here, we present a novel method for assessing CEC function through morphological analysis. Using machine learning, we extract cellular features from corneal endothelial images and quantify shape distortion via a geometric-based metric—the CEC Xin-Value (XV). Validated for accuracy and functional relevance, the XV enables a refined, image-driven Corneal Endothelial Evaluation System (CEE-System) that integrates cell density, morphology, and functional cell subtype distribution across damage stages. It serves as an effective tool for clinical specialists, facilitating the assessment of CEC function and opening new avenues for image-based cell function analysis.

Results

Single-cell level data extraction of corneal endothelium

The central analysis method, commonly used in clinical practice, captures five corneal endothelial images and computes ECD, CV, and HEX for diagnostic reference (Fig. 1). We evaluated these parameters across patient groups with varying ECD and central corneal thickness (CCT). No significant differences in CV or HEX were found between groups. ECD differed significantly in most comparisons, except between clear cornea with low ECD (CC-LD) and corneal edema with low ECD (CE-LD); CCT showed similar trends, with nonsignificant differences between CC-LD – clear cornea with high ECD (CC-HD) and CE-LD – corneal edema with high ECD (CE-HD) (Supplementary Fig. 1). These results indicate that the conventional central analysis method is limited in assessing CEC function based on the morphology.

To establish a precise digital method for CEC functional assessment, we developed an accessible Image-based Recognition and Data Extraction (IRDE) tool using clinical corneal endothelial single-cell imaging data (Fig. 1). Following corneal endothelial microscopy, raw images and central analysis data were collected. Based on established methodologies[22–24], the raw images were processed using automated image recognition and segmentation algorithms, generating a Voronoi diagram with precise vertex coordinates for each endothelial cell. Custom scripts accessed vertex data to accurately delineate polygonal cell boundaries. The software's built-in ANSYS parametric design language enabled systematic traversal of each cell, extracting detailed morphological parameters—including side length, perimeter, diagonal length, internal angles, and cell area. It also autonomously computed key metrics such as ECD, mean cell area, and standard deviation for whole-image quantitative analysis. This approach provides robust, high-resolution morphological data essential for accurate, image-driven evaluation of CEC function.

Development of the Xin-value analysis method: a novel parameter for evaluating CEC function

Our previous research demonstrated that changes in CEC diagonals reflect cell function[25]. Diagonal variation indicates the extent of geometric distortion in polygonal cells, while average CEC area inversely correlates with cell density. Building on these findings, this study integrates patterns of diagonal and area changes in CEC morphology to develop a novel calculation method for XV—a new metric designed to quantify morphological distortion in CECs, which is defined in Eq. (1):

$$XV = \frac{S}{S_{th}} \times \frac{D_{\max}}{D_{\min}} \tag{1}$$

Where S is the area of a single cell, S_{th} is the critical cell area threshold at functional decompensation, $D_{\max}$ is the longest diagonal, and $D_{\min}$ is the shortest diagonal. Using geometric modeling of corneal endothelial images, we derived $D_{\max}$, $D_{\min}$, and S via script execution to transform the original CEC map into visualized XV images (Fig. 2). In post-PK patients with endothelial dysfunction (ECD: 400–700 cells/mm²) at Qingdao Eye Hospital of Shandong First Medical University, the average cell area plateaued at 2854.41 μm²—designated as S_{th}.

Geometrically, aberration quantifies deviation from an ideal polygonal shape: in hexagons, this includes distortions in diagonal ratios, side lengths, angles, and area. To validate the XV formula's accuracy in capturing shape distortion, we developed the Polygon_Piecewise application. For simplification, we set D_{max} = D, D_{min} = d, and treated S_{th} as a constant, effectively normalizing its influence, yielding Eq. (2):

$$XV = S \times \frac{D}{d} \tag{2}$$

Assuming that the side length of the square hexagon is 1, the square hexagonal product S_0 and $\frac{D_0}{d_0}$ are as follows Eqs. (3) and (4) :

$$S_0 = \frac{3\sqrt{3}}{2} \approx 2.60 \tag{3}$$

$$\frac{D_0}{d_0} = \frac{2}{\sqrt{3}} \approx 1.15 \tag{4}$$

As illustrated in Fig. 2, changes in cell morphology altered parameters such as cell area, edge count, and perimeter, leading to corresponding shifts in the XV, which is determined by variations in both area and diagonal ratios (Supplementary Table 1). XV increases proportionally with cell area and diagonal ratio; furthermore, changes in the number of cell edges also influence the XV (Supplementary Fig. 2a, b). Thus, the XV effectively captures morphological deviations in CEC shape and size, providing a reliable metric for assessing cellular function through morphological alterations.

The changes in CEC XV reflect the cellular function

To investigate the relationship between CEC function and the XV, we employed three distinct animal models of corneal endothelial decompensation: the Col8a2^{Q455K} mouse model, the UVA-induced mouse model, and the rabbit corneal endothelial cryoinjury model. In mouse models, Tom20 expression was significantly reduced ($^{*}P < 0.05$, $^{**}P < 0.01$), indicating mitochondrial dysfunction during decompensation. Cells with lower Tom20 showed higher XV, with strong negative correlations observed (R = −0.6328, $^{***}P < 0.001$ in the UVA model; R = −0.7014, $^{***}P < 0.001$ in the Col8a2^{Q455K} model, Fig. 3a–c), indicating that mitochondrial dysfunction is closely associated with morphological stress at the single-cell level.

To evaluate cellular stress responses, we analyzed the expression of stress markers in the UVA model. Hsp70 and γ-h2AX signals were significantly elevated (both $^{**}P < 0.01$), indicating protein stress and DNA damage (Fig. 3d, e). Notably, both markers showed strong positive correlations with XV (Hsp70 vs. XV: R = 0.8676, γ-h2AX vs. XV: R = 0.9555, Fig. 3f), confirming that increased XV reflects heightened cellular stress.

To investigate the relationship between CEC XV and cellular function, we established a rabbit corneal endothelial cryoinjury model to monitor dynamic XV changes during cell damage and recovery. In the rabbit cryoinjury model, corneas developed edema and opacity post-injury, with alizarin red staining showing central cell loss and peripheral morphological changes. Over 14 days, transparency and thickness recovered, paralleling a decline in mean XV, which inversely correlated with ECD and CCT (Fig. 3g, h). These findings consistently demonstrate that XV reflects mitochondrial function, cellular stress, and functional recovery, establishing it as a sensitive, morphology-based biomarker of CEC dysfunction.

Comprehensive evaluation of the clinical diagnostic efficacy of XV

We analyzed the consistency between parameters extracted using the IRDE approach and those obtained through the traditional central analysis method (Supplementary Fig. 3 and Supplementary Table 2). To evaluate the diagnostic efficacy of XV, we performed a systematic comparison of XV, ECD, CV, and their combinations-including composite indices (e.g., ECD/CV, ECD × HEX/CV)-using linear discriminant analysis (LDA) with

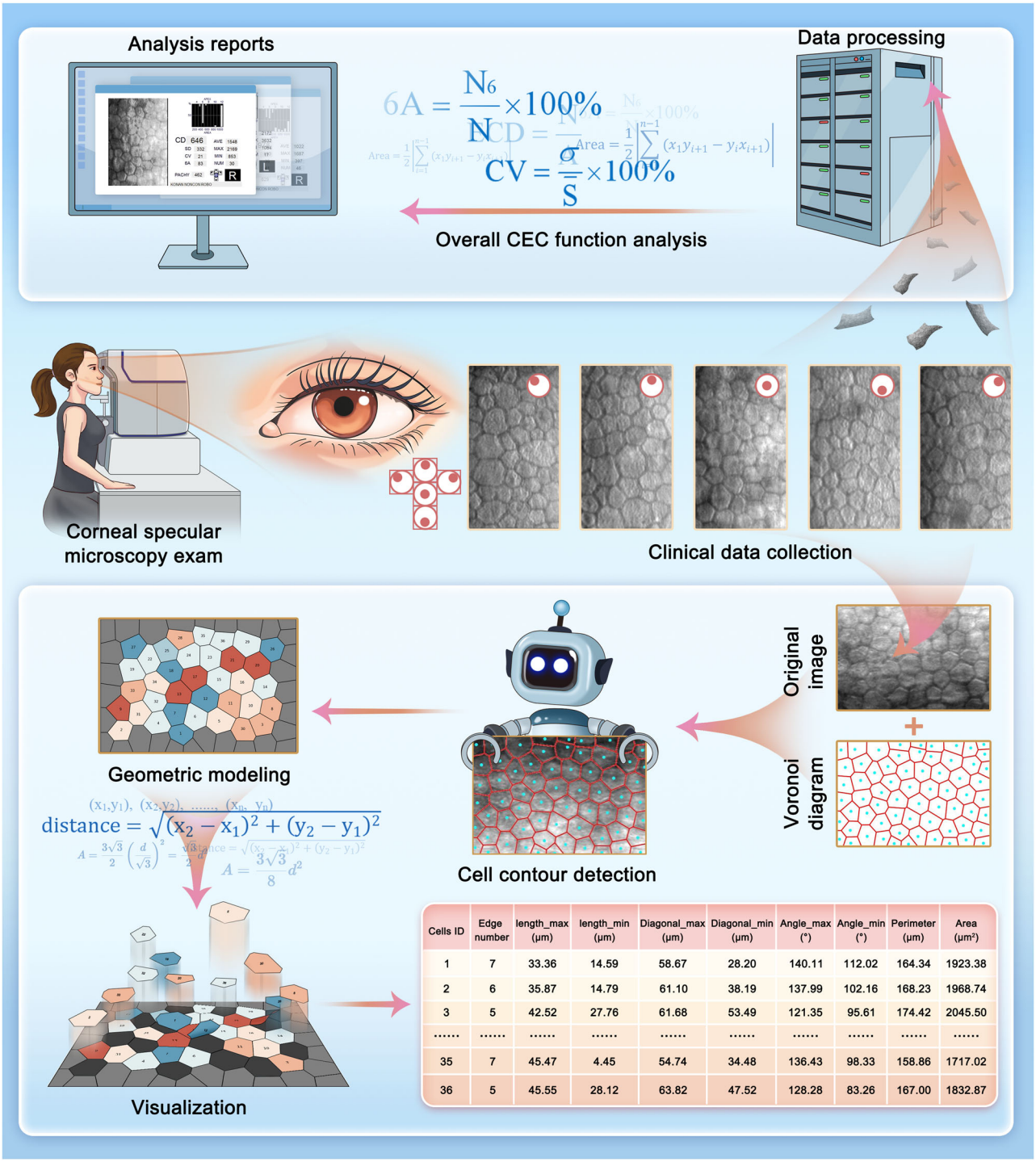

Cells ID	Edge number	length_max (μm)	length_min (μm)	Diagonal_max (μm)	Diagonal_min (μm)	Angle_max (°)	Angle_min (°)	Perimeter (μm)	Area (μm²)
1	7	33.36	14.59	58.67	28.20	140.11	112.02	164.34	1923.38
2	6	35.87	14.79	61.10	38.19	137.99	102.16	168.23	1968.74
3	5	42.52	27.76	61.68	53.49	121.35	95.61	174.42	2045.50
.....	.....	.....	.....	.....	.....	.....	.....	.....	.....
35	7	45.47	4.45	54.74	34.48	136.43	98.33	158.86	1717.02
36	5	45.55	28.12	63.82	47.52	128.28	83.26	167.00	1832.87

Fig. 1 | Workflow of CECs image recognition and IRDE tool. Following endothelial microscopy, raw images and central analysis results were obtained. Images underwent segmentation and processing using image recognition algorithms to produce a Voronoi diagram, serving as a basis for geometric modeling. Morphological parameters were then extracted at the single-cell level and across the entire image using the software.

10-fold cross-validation. Performance was assessed by overall accuracy, sensitivity, and specificity across all possible parameter combinations. Comparison of XV and CV between normal and abnormal conditions. The area under the curve (AUC) was 1.0 (95% CI: 1.0–1.0), with both sensitivity and specificity at 1.0 ($^{***}P < 0.001$). The CV was 0.523 (95% CI: 0.426–0.620), with a sensitivity of 0.186 and specificity of 0.253 ($P = 0.678$). XV comparison between CC-PK and CE-PK groups revealed an AUC of 0.796 (95% CI:0.722–0.871), with a sensitivity of 0.764 and specificity of 0.681 ($P < 0.001$). The CV was 0.687 (95% CI: 0.594–0.780), demonstrating a sensitivity of 0.455 and specificity of 0.824 ($^{***}P < 0.001$) (Fig. 4a). As shown in Table 1 and Supplementary Table 3, XV outperformed all single parameters, achieving the highest classification accuracy (0.776, 95% CI:0.708–0.831), surpassing ECD (0.753, 95% CI:0.684–0.811). Notably, traditional composite indices showed limited diagnostic gain and, in some cases, performed worse than ECD alone, highlighting their suboptimal utility in clinical decision-making. Most importantly, the combination of XV and CCT achieved very high classification accuracy (0.977, 95% CI:0.942–0.991), with both sensitivity and specificity approaching 1.00.

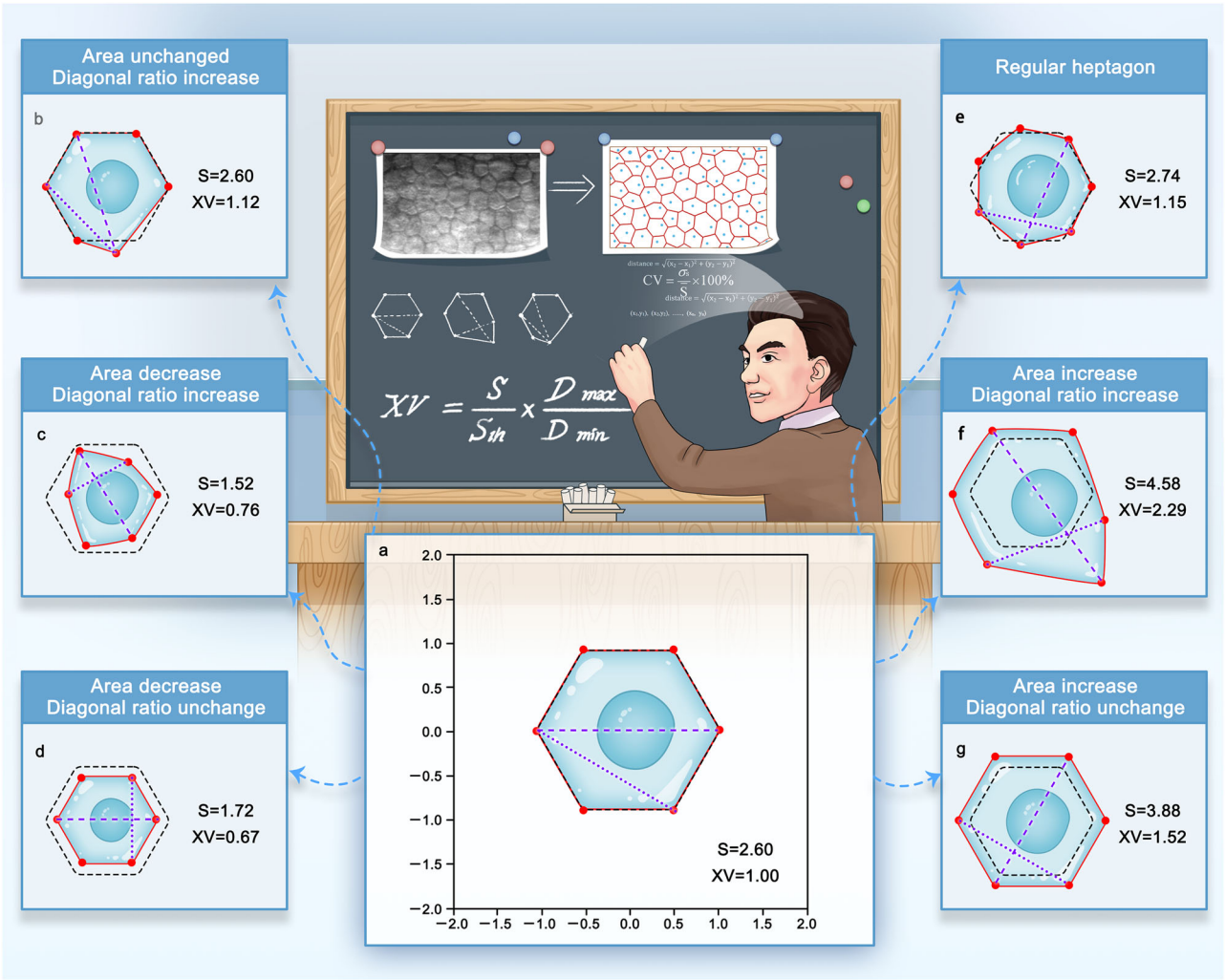

Fig. 2 | Geometric analysis and validation of the XV. Geometric data were extracted from corneal endothelial images to calculate and visualize the XV metric. **a** Assuming a hexagonal area (S) of 2.60, XV was defined as 1.00. Variations in the hexagonal area and diagonal ratios demonstrate differential effects on XV; **b** An increase in the diagonal ratio at constant area results in a higher XV; **c** Reductions in both area and diagonal ratio further diminish XV; **d** A constant diagonal ratio with a decreasing area results in a lower XV; **e** Additionally, XV shows a direct proportional relationship with side length, indicating that longer side lengths correspond to higher XV; **f** Simultaneous increases in both area and diagonal ratio yield a substantial rise in XV; **g** An increase in the area at constant diagonal ratio results in a higher XV.

This synergistic effect underscores XV's ability to capture early morpho-functional changes that precede measurable thickening, making the XV × CCT pair a highly promising, minimal yet maximally informative biomarker panel for clinical use. These results suggest that XV provides incremental value over conventional morphometric parameters and complements structural metrics such as CCT in the assessment of endothelial function. The improved diagnostic performance when combining XV with existing indices supports its potential for more comprehensive evaluation of corneal endothelial health.

Analysis of the CEC characteristics under normal and pathological conditions using XV

To evaluate the clinical utility of the XV, we colleted the data from 155 normal and 155 corneal endothelial decompensated patients. The mean XV in normal corneas (XVn_th) was 0.274 (95% CI:0.270–0.277), significantly lower than the decompensated group's mean (XV_{d_th}) of 1.497 (95% CI:1.456–1.538; $P < 0.001$) (Fig. 4b, c). While prior studies rely on ECD to assess damage[26], we performed single-cell XV analysis on 3,984 cells from 73 images across varying ECD zones, revealing a strong inverse correlation between ECD and XV (Fig. 4d). At ECD > 2000 cells/mm², 71.4% of cells had XV < 0.274, and none exceeded 1.497. As ECD declined, the proportion of high-XV cells increased: at 1000–2000 cells/mm², 0.3% exceeded 1.497; at 500–1000, 7.2%; at 300–500, 41.2%; and at <300, 83.8% surpassed 1.497, with none below 0.274 (Fig. 4e). These findings demonstrate that XV increases with endothelial stress and functional decline. We integrated XV distribution patterns into the existing corneal endothelial damage classification, refining the grading system (Table 2) and establishing the XV-based Corneal Endothelial Evaluation System (CEE-System) for single-cell functional assessment. This enhanced framework enables the morphology-driven evaluation of corneal endothelial function across disease stages.

Clinical application of the XV-Based CEE-System

To validate the clinical applicability of the XV–based CEE-System, we developed a standardized workflow (Fig. 5a). Patients underwent corneal endothelial microscopy, and images were analyzed by the CEE-System to assign a functional grade, which was then compared with expert clinician assessments. We selected 150 images—30 from each CEE-System grade (I–V)—and blinded nine ophthalmologists, stratified by clinical experience (junior: <5 years; intermediate: 6–10 years; senior: >10 years), to independently assign grades. Junior ophthalmologists achieved an overall accuracy of 0.42 relative to the CEE-System, with grade-specific correct rates of 0.51, 0.29, 0.35, 0.41, and 0.76 (Fig. 5b, e). Intermediate ophthalmologists showed

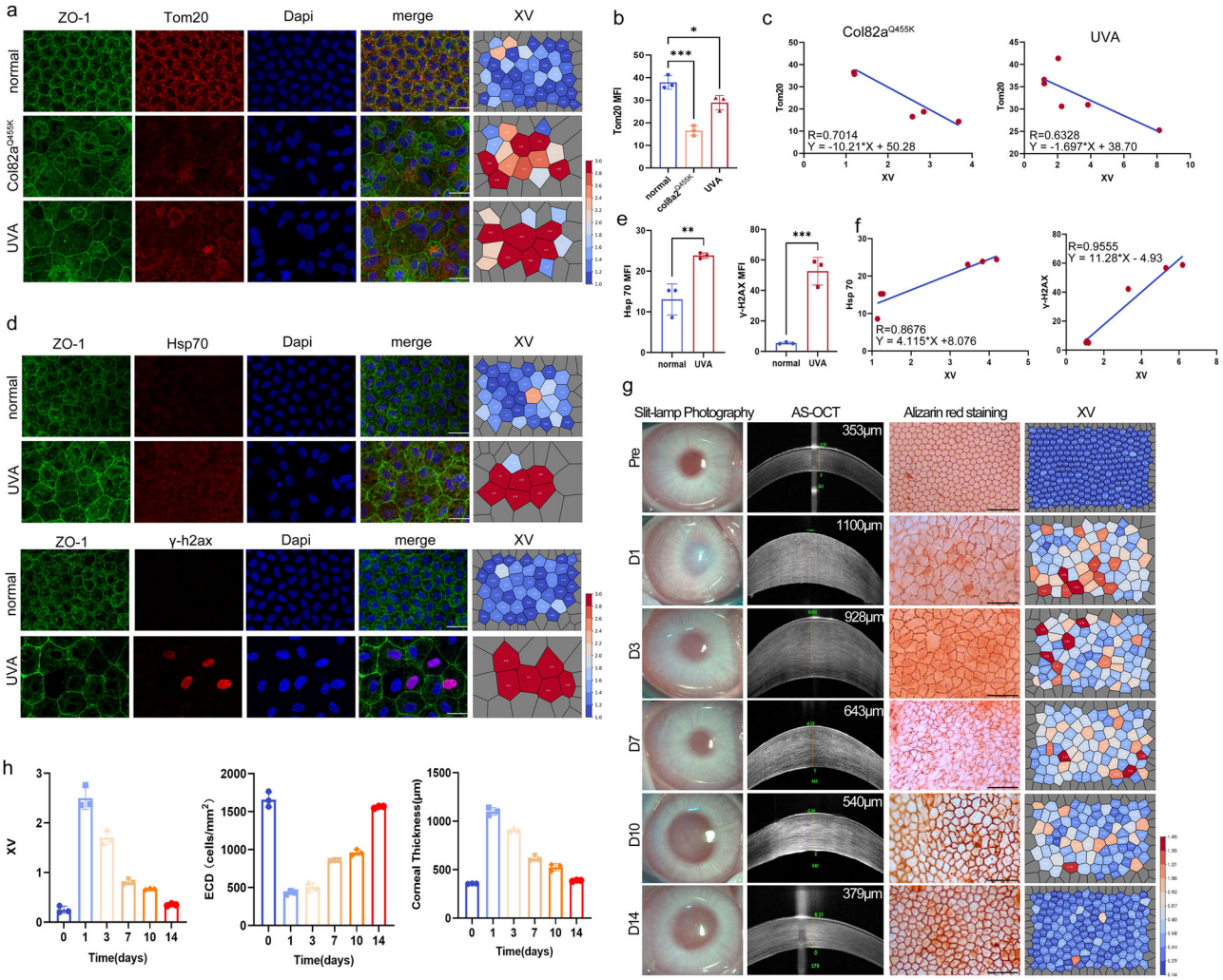

Fig. 3 | The changes in CEC XV reflect the cellular function. **a** Immunofluorenscence staining of ZO-1 (green), Tom20 (red), and corresponding XV visualization in normal and conreal endothelial dysfunction mouse models. **b** Tom20 expression of Col8a2^{Q455K} mouse model and UVA-induced mouse model were significantly reduced ($^{*}P < 0.05$, $^{***}P < 0.001$). **c** Both markers showed significant negative correlations with XV. **d** Immunofluorenscence staining of ZO-1 (green), Hsp70 (red), γ-H2AX (red), and corresponding XV visualization in normal and UVA-induced corneal endothelial dysfunction mouse models. **e** Hsp70 and γ-H2AX exhibited increased fluorescence intensity with rising XV ($^{**}P < 0.01$, $^{***}P < 0.001$). **f** Both markers showed significant positive correlations with XV. **g** Slit lamp photography, corneal thickness changes, Alizarin red staining of the endothelium, and XV visualization in rabbits at different time points post-cryoinjury. **h** Mean XV peaked on the first-day post-cryoinjury, gradually decreasing over time until returning to preoperative values. The central region of the corneal endothelium exhibited significant damage and low cell density after cryoinjury; however, regeneration restored endothelial cell density to preoperative levels over time corneal thickness peaked on the first-day post-cryoinjury and gradually decreased to preoperative levels. (bar = 50 μm, $n = 3$).

improved overall accuracy (0.50), with higher agreement in grades 3–4 (0.47–0.54 vs. 0.35–0.41), while grades 1, 2, and 5 remained comparable (Fig. 5c, e). Senior clinicians achieved the highest overall diagnostic accuracy (0.54), with stage-specific accuracies of 0.47, 0.24, 0.47, 0.65, and 0.97 for disease stages 1 to 5, respectively. The marked increase in accuracy at advanced stages (grades 4–5) reflects the greater visibility of endothelial abnormalities—such as severe cell loss and pleomorphism—that facilitate clinical judgment. This pattern highlights the challenges in diagnosing early-stage dysfunction, even among experienced observers (Fig. 5d, e). Notably, all groups showed lower accuracy in grade 2, suggesting diagnostic ambiguity in early-moderate dysfunction. The CEE-System's quantification and standardization can effectively assist doctors at all grades in evaluating the function of damaged CECs.

To test broader applicability, we applied XV analysis to non-endothelial cells. In corneal epithelial confocal images, diabetic keratopathy and viral keratitis patients exhibited significantly higher XV than healthy controls ($P < 0.001$; Supplementary Fig. 4a). In retinal pigment epithelial (RPE) cells, ZO-1 stained images from retinal degenerative RCS rats showed enlarged, irregular cells with significantly increased XV compared to normal SD rats ($P < 0.01$; Supplementary Fig. 4b). These results confirm that pathological stress induces morphological distortion across diverse cell types with regular packing. Thus, quantifying shape aberration via XV provides a universal, morphology-based proxy for cellular function, extending the CEE-System's potential beyond corneal endothelium to other structured epithelium.

Discussion

Corneal endothelial specular microscopy is essential for clinical assessment but limited in functional evaluation and early diagnosis of endothelial dysfunction. This study introduces a novel, single-cell-level approach that enables digital transformation of corneal endothelial imaging through integration of machine learning, geometric modeling, and biochemical principles. The XV represents a morphometric approach that captures subclinical changes in CECs with higher sensitivity than traditional ensemble metrics such as CV, CCT, and ECD. Within the XV-optimized CEE-System, this parameter supports a more comprehensive and cell-

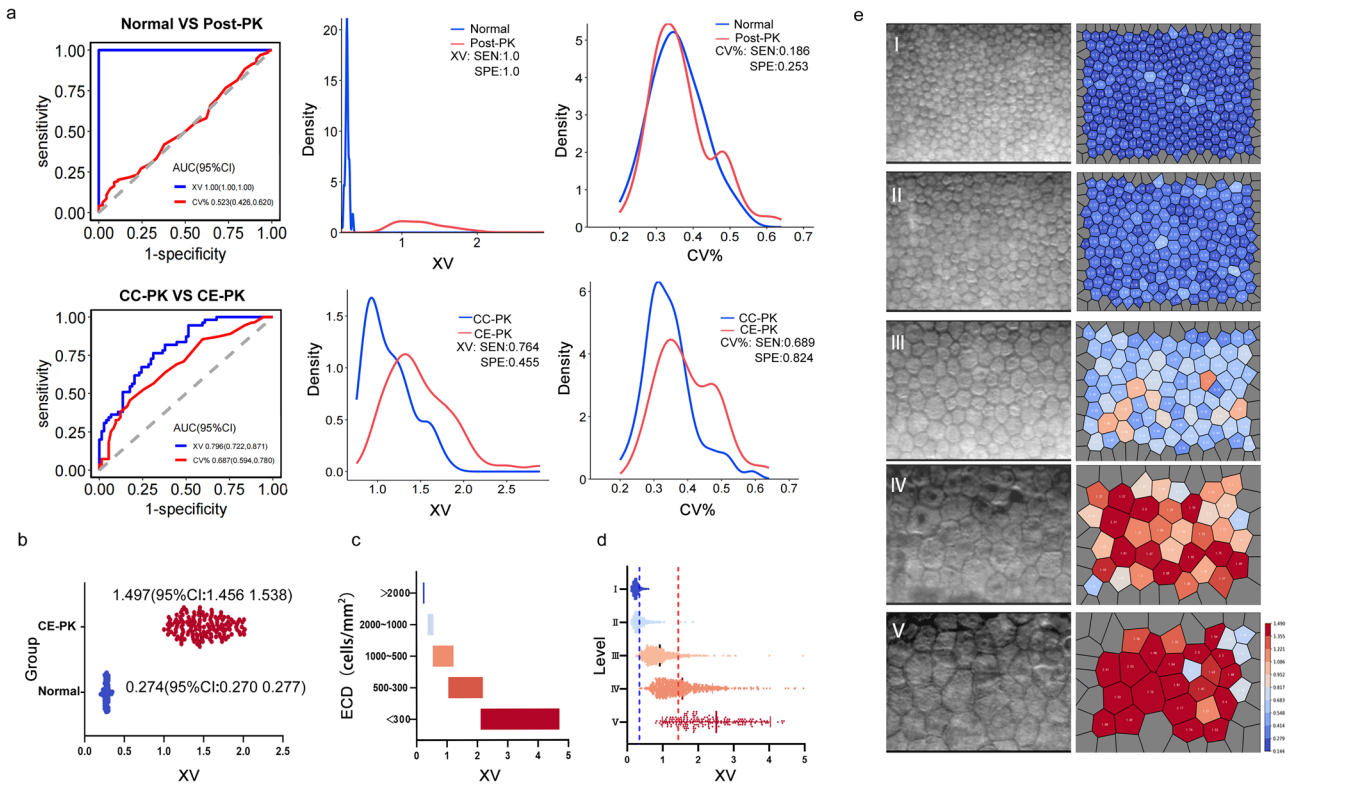

Fig. 4 | Evaluation of corneal endothelial cell XV testing efficiency across various conditions and establishment of an XV-based assessment system. a Comparison of XV between normal and abnormal conditions. The AUC was 1.0 (95% CI: 1.0–1.0), with both sensitivity and specificity at 1.0 (***$P < 0.001$). The CV was 0.523 (95% CI: 0.426–0.620), with a sensitivity of 0.186 and specificity of 0.253 ($P = 0.678$). XV comparison between CC-PK and CE-PK groups revealed an AUC of 0.796 (95% CI: 0.722–0.871), with a sensitivity of 0.764 and specificity of 0.681 (***$P < 0.001$). The CV was 0.687 (95% CI: 0.594–0.780), demonstrating a sensitivity of 0.455 and specificity of 0.824 (***$P < 0.001$). **b** Mean XV in normal versus decompensated groups. **c** Changes in corneal density and XV at various postoperative intervals following PK. **d** Grading of CEC function based on XV, with a threshold of 0.27 indicated by the blue line and 1.49 by the red line. **e** Illustrative examples of corneal endothelial cell function grades I to V.

Table 1 | Comparison of diagnostic performance of individual parameters

Variable	Accuracy (95%CI)	Sensitivity			Specificity		
		CC-PK vs other	CE-PK vs other	Normal vs other	CC-PK vs other	CE-PK vs other	Normal vs other
XV	0.776 (0.708, 0.831)	0.824	0.527	1.000	0.740	0.891	1.000
ECD	0.753 (0.684, 0.811)	0.757	0.545	1.000	0.750	0.849	1.000
ECD*HEX/CV	0.747 (0.678, 0.806)	0.919	0.236	0.956	0.560	0.950	1.000
CD/CV	0.712 (0.641, 0.775)	0.892	0.364	0.978	0.640	0.933	1.000
CCT	0.707 (0.635, 0.769)	0.919	1.000	0.000	0.560	0.950	0.992
CV	0.489 (0.415, 0.562)	0.838	0.418	0.000	0.350	0.798	1.000
HEX	0.471 (0.399, 0.545)	0.811	0.364	0.044	0.270	0.866	0.977

Table 2 | XV-based functional grading of CEE-System

Grade	CD (cells/mm²)	XV	<XV_{n_th} (%)	å XV_{d_th} (%)	Annotation
I	> 2000	0.2~0.28	>71.4%	0	Normal function
II	2000-1000	0.28~0.43	71.4~11.4%	0~0.3%	Below normal physiological conditions
III	1000-500	0.43~1.40	<11.4%	0.3~7.2%	Impaired corneal endothelial function, clinically insignificant
IV	500-300	1.40~2.67	0	7.2~41.2%	Inner eye surgery may lead to bullous corneal lesions
V	<300	> 2.67	0	> 41.2%	Has already developed or is highly susceptible to bullous corneal lesions

resolved framework for monitoring endothelial health and functional decline. This advancement enhances precision in detecting early corneal endothelial damage, offering significant clinical potential for the timely diagnosis and management of corneal endothelial pathologies.

Currently, no standardized protocol exists for comprehensive clinical assessment of CECs[27]. Routine evaluation relies on corneal transparency and thickness as surrogate markers of endothelial function—parameters that remain normal until significant cell dysfunction has already occurred. By the

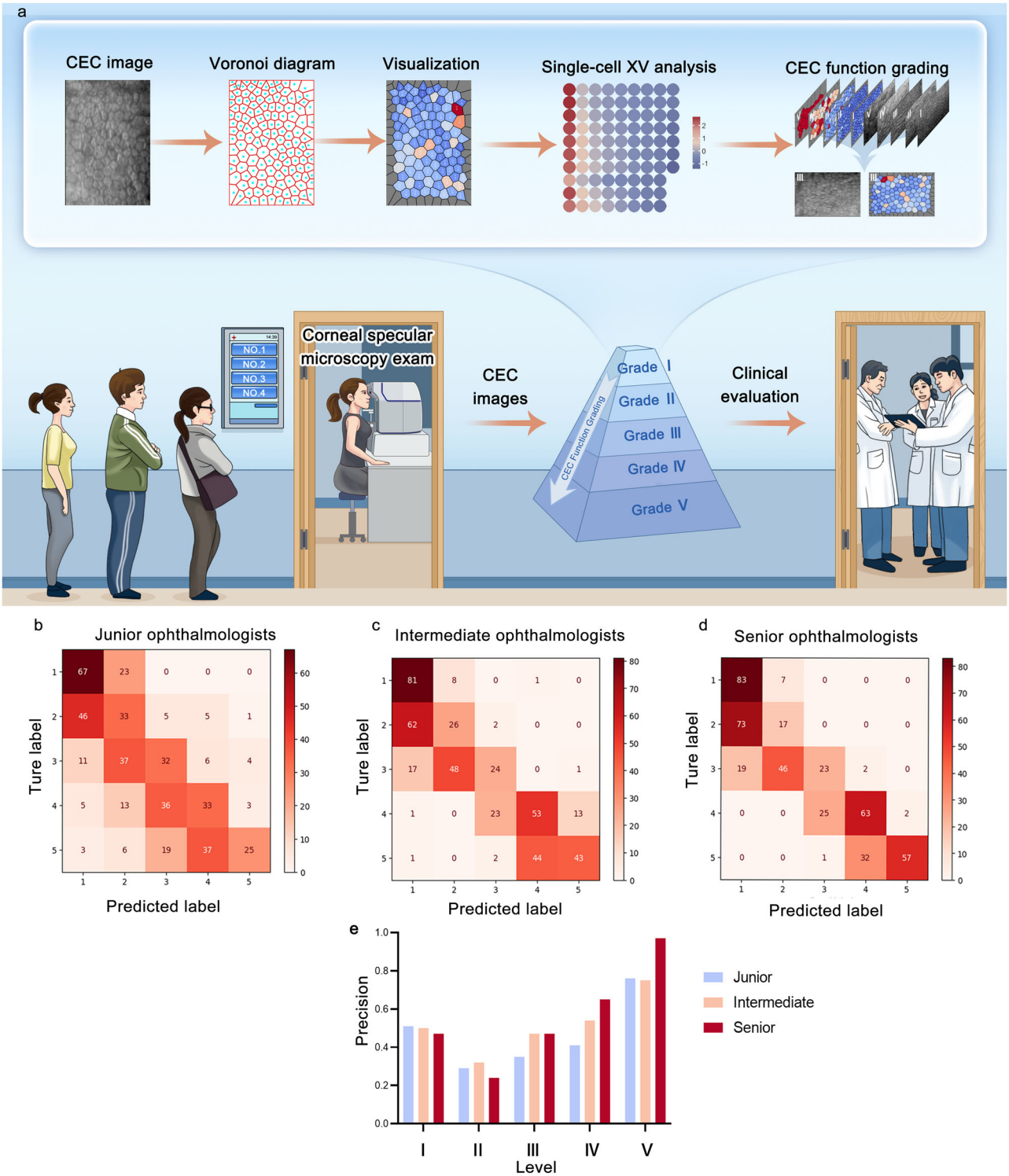

Fig. 5 | Corneal endothelial function grading system based on XV. a Overview of the workflow for the CEE-System. **b** Performance of junior ophthalmologists in grading endothelial function, demonstrating a precision of 0.42 when compared to the CEE-System. Accuracy rates for patient functional assessments across the five grades were 0.51, 0.29, 0.35, 0.41, and 0.76, respectively. **c** Intermediate ophthalmologists achieved a precision of 0.50 relative to the CEE-System, with accuracy rates of 0.50, 0.32, 0.47, 0.54, and 0.75 for the five grades. **d** Advanced ophthalmologists showed a precision of 0.54 compared to the CEE-System, with accuracy rates of 0.47, 0.24, 0.47, 0.65, and 0.97 across the five grades. **e** Comparative analysis of accuracy rates among the three clinician groups at all grading levels against the CEE-System.

time edema or clouding appears, irreversible damage is often present, limiting early intervention[2]. Clinically, assessment is largely confined to overall metrics such as ECD, HEX, and CV[7,28]. Although advances in AI have enhanced image segmentation and recognition in ophthalmology, applications for precise CEC functional diagnosis remain underdeveloped[9–13]. In this study, we established a single-cell level analytical framework by integrating machine learning with geometric modeling of clinical endothelial images. Our approach extracts detailed morphological

features—including cell areas, angles, side lengths, and diagonals—enabling high-resolution analysis beyond conventional parameters. This comprehensive data integration allows for granular, image-based evaluation of individual CEC morphology and function.

Recent study suggests CEC volume may also be informative[29]. Molecular approaches like multi-omics or biological probes offer functional insights but are limited by invasiveness and sampling challenges[30]. Notably, Professor Shigeru Kinoshita's group demonstrated that in vitro expansion of donor-derived endothelial cells can predict post-transplant CEC survival, highlighting a promising ex vivo strategy for functional assessment[31]. But these metrics collectively fail to capture true functional status. Importantly, high XV were associated with decreased expression of Tom20, a mitochondrial marker, suggesting a link between morphological deviation and cellular metabolic activity. Moreover, XV showed strong positive correlations with Hsp70 and γ-H2AX, confirming that the increased XV reflects heightened cellular stress. In a cryoinjury animal model, XV trends correlated with recovery in ECD, CCT, and transparency. Therefore, our findings indicate that XV serves as an indirect sensitive indicator of single-cell functional state. Moreover, the diagnostic model incorporating XV achieved higher accuracy (97.7%) when combined with CCT, outperforming models based on ECD, CV, or their combinations. While the absolute gains were modest, these results suggest that cell-level morphometric analysis may contribute additional information for detecting endothelial dysfunction. While XV shows strong correlation with ECD at the global level, it emerges from a fundamentally different analytical framework—one based on single-cell morphometric profiling rather than averaged density. This approach may enable future investigations into cellular heterogeneity and localized dysfunction, aspects that remain invisible to standard clinical metrics. Although the current diagnostic improvement is marginal, the value of XV may lie not only in its incremental statistical performance but also in its potential to support granular, cell-resolved analyses that could inform mechanistic studies or personalized monitoring strategies.

Current clinical methods for evaluating CECs often delay or miss early pathology detection, leaving corneal transplantation as the primary intervention[2]. In 2014, the Japanese Corneal Disease Society established a five-tier grading system based solely on cell density, offering limited clinical insight despite aiding classification[26]. Corneal endothelial imaging provides rich morphological data beyond density[7]. In this study, we analyzed CEC images across clinical states—from normal to post-transplant decompensation—assessing XV distribution and functional cell proportions.We refined the traditional grading system into a comprehensive CEE-System that incorporates cell quantity, morphology, and functional heterogeneity. Clinical validation showed that the XV-based model achieved higher sensitivity in identifying early signs of endothelial dysfunction in morphologically borderline or asymptomatic corneas, suggesting its potential to detect subclinical changes before they become evident with conventional metrics. Notably, XV also distinguished pathological states in corneal epithelial confocal images, and correlated with damage severity in RPE cells in models of retinal degeneration. These findings suggest morphological distortion, quantified by XV, may serve as a universal proxy for cellular function.

This study established a novel single-cell evaluation method for CEC function and refined the grading system for endothelial damage, advancing clinical diagnosis. However, limitations remain: (1) While machine learning enabled automated image recognition, manual annotation still enhances accuracy future work should achieve fully automated, high-precision analysis. (2) The XV leverages geometric principles—cell area and diagonals—to quantify shape distortion and infer function. Incorporating additional morphological features (e.g., angles, side lengths) could improve sensitivity, and in vitro assays should validate the XV–function relationship. (3) The model was developed and tested using images from healthy individuals and post-transplant patients. Expanding to diverse corneal pathologies and increasing the dataset size would strengthen generalizability. Addressing these limitations will further enhance the accuracy, robustness, and clinical utility of the XV-based CEE-System across a broader spectrum of corneal endothelial diseases. (4) Although XV offers the advantage of single-cell functional assessment, its potential in corneal endothelial cell function assessment and disease diagnosis remains to be fully explored and will require further clinical data and validation for a more comprehensive evaluation.

In conclusion, our findings confirm that alterations in CEC morphology reflect cellular function. We developed the XV to assess cell function at the single-cell level and refined a clinically relevant grading system based on XV. This framework enables early detection and monitoring of corneal endothelial dysfunction and offers broad potential for image-based functional assessment of polygonal cell types, advancing both research and clinical practice in ophthalmology.

Methods

Image datasets

Original and analyzed images of the corneal endothelium were collected from selected patients at Qingdao Eye Hospital of Shandong First Medical University, between March 2017 and December 2023. The CEC images for all patients were captured using the NSP-9900 II corneal endothelial microscope of KONAN, Japan. Exam parameters included a photographic field of view of 0.24 mm × 0.4 mm and a photographic magnification of 308 (8.4-inch monitor). The photograph was taken in the center of the corneal endothelial cell image, and the centroid method procedure was used to analyze at least 30 consecutive countable cells[32]. Low-quality images characterized by halos, astigmatism, and insufficient lighting were excluded as they resulted in challenges in image recognition. The study procedure adhered to the requirements of the Declaration of Helsinki. The study was registered with ClinicalTrials.gov (ChiCTR2400088994).

Model construction

According to established methodologies[22,23], IRDE tool was developed tailored to clinical CEC images. Histogram equalization was applied to convert the original image to grayscale, adaptive window filtering was used for denoising and threshold calculation. Subsequent steps included image processing through hole-filling algorithms and erosion operations after threshold segmentation. Based on the segmented image, the cell's centroid was calculated for precise positioning and marking. Automatic identification of errors in the image was conducted to ensure accuracy, followed by manual alterations involving the addition or deletion of centroids. Finally, a Voronoi diagram was generated by the system, utilizing the centroid data along with the original image information, and the coordinate data was saved as a JSON file.

As a standard, the Voronoi diagram generated by image recognition was used to construct the geometric model. Following the output of each cell's vertex coordinates by image recognition, a script was written using the software Ansys Apdl (version 15.0) to read the vertex coordinate information and identify the polygonal cell boundaries. After the image was geometrically modeled, the polygons could be connected[24].

After geometric modeling, the api that comes with the software was used to traverse each cell and measure the side length, perimeter, diagonal length, interior angle, and area of each cell. Cells with incomplete outermost rings were excluded from the measurements.

Using the vertex coordinates of the polygon, its area was calculated using Shoelace's formula. Assuming that the vertices of the polygon are (x_1,y_1), (x_2,y_2), ……, (x_n, y_n), the area can be calculated using the following Eq. (5):

$$A = \frac{1}{2}\left|\sum_{i=1}^{n-1}(x_1 y_{i+1} - y_i x_{i+1}) + (x_n y_1 - x_1 y_n)\right| \quad (5)$$

The distance between the current node and other nodes was calculated using the Euclidean distance formula, iterating over all nodes (points on the same edge are not counted). The formula for calculating distance between

two points, x_1, y_1, and x_2, y_2, as shown in Eq. (6):

$$d = \sqrt{(x_2 - x_1)^2 + (y_2 - y_1)^2} \quad (6)$$

The maximum and minimum values in the result of the calculation were the longest and shortest diagonals, respectively.

However, edge cells are only partially visible, and their true area cannot be accurately determined, which will introduce bias into both cell morphometric and density measurements. Therefore, the formula for calculating ECD used in this study is as shown in Eq. (7):

$$ECD = \frac{N_{inner}}{Area_{inner}} \quad (7)$$

N_{inner} refers to the number of non-edge cells. $Area_{inner}$ refers to the total area of non-edge cells.

All non-edge cells are fully contained within the field of view, ensuring accurate segmentation and area measurement. The cell boundaries used for area calculation are derived from the Voronoi tessellation generated based on geometrically detected cell centers (via distance transform), which reconstructs the complete cellular mosaic even in densely packed or irregular monolayers.

Data analysis

A total of 174 original images of CECs were selected and divided into three groups based on the central method reported in the results: (1). CC-PK Group: 74 images from 74 cases of post-PK with ECD of 400–1000 cells/mm^2 and CT < 620 μm. (2). CE-PK Group: 55 images from 55 cases of post-PK with ECD of 400–1000 cells/mm^2 and CT > 620 μm. (3). Normal Group: 45 images from 45 cases with ECD of 2500-3000 cells/mm^2 and CT ≤ 620 μm. These images were used to verify the accuracy of data extracted by the IRDE tool and to analyze the diagnostic efficacy of the XV in different disease conditions. A total of 310 original CEC images were selected from 310 cases, comprising 184 males and 126 females. The ECD values extracted using the IRDE system were categorized into two groups: (1) CE-PK group: 155 cases with ECD ranging from 400 to 1000 cells/mm^2, and (2) Normal group: 155 cases with ECD ranging from 2500 to 3000 cells/mm^2. This classification facilitated the critical value analysis of XV in both normal and dysfunctional corneal endothelium. A total of 73 cases with 73 original CEC images and 3983 cells were selected for analysis. The cases were divided into five groups according to the ECD values extracted from the IRDE tool: (1) ECD > 2000 cells/mm^2, represented by 5 images comprising 981 cells; (2) ECD between 1000 and 2000 cells/mm^2, represented by 10 images comprising 1141 cells; (3) ECD between 500 and 1000 cells/mm^2, represented by 17 images comprising 877 cells; (4) ECD between 300 and 500 cells/mm^2, represented by 27 images comprising 765 cells; and (5) ECD < 300 cells/mm^2, represented by 14 images comprising 216 cells. The single-cell XV was extracted and analyzed to characterize the XV distribution of CEC across different functional stages, contributing to the development of the CEE-System. A total of 150 CEC images were selected, with 30 images representing each of the five grades (I-V) as determined by the CEE-System analysis. Nine practicing ophthalmologists from the Department of Corneal Disease at Qingdao Eye Hospital of Shandong First Medical University participated in the study. They were divided into three distinct groups based on their years of experience: the junior group with less than 5 years of experience in diagnosing and treating corneal diseases; the intermediate group with 6 to 10 years of experience; and the senior group with over 10 years of experience in the same field. Each ophthalmologist independently graded the functional status of each image, relying solely on the image information without any additional clinical context. In this research, we utilized the corneal endothelial damage grading system, developed by the Japanese Corneal Disease Society and based on cell density[26], as the reference standard. We performed a correlation analysis between this grading system and the CEE-System's endothelial function grading. Additionally, we assessed the accuracy of functional evaluations conducted by three groups of clinicians, comparing their results with the CEE-System's endothelial function grading.

Furthermore, corneal epithelial images obtained using a laser confocal microscope (HRT3, Heidelberg, Germany) were chosen from a total of 9 cases and 9 images. Among these, 3 cases and 3 images were identified as having herpes simplex keratitis (HSK) during outpatient evaluations, 3 cases and 3 images were associated with diabetic keratopathy, and the remaining 3 cases and 3 images were sourced from a normal control group. The images were processed to extract XV using the IDRE system, followed by an analysis of changes in XV across various diseases.

Basic experimental methods

Healthy New Zealand white rabbits (3–4 months old, male, weighing 2.0–2.5 kg), C57 mice (6–8 weeks old, female), Sprague-Dawley (SD) rats (6–8 weeks old, male) without visible ocular or systemic abnormalities were purchased from Jinan Xilingjiao Breeding Company (Jinan, China) and Shandong Taike Biotechnology Co., Ltd. (Jinan, China). Col8a2^{Q455K} mice (6 months old, female) were obtained from Jackson Laboratory (Bar Harbor, ME, USA). Royal College of Surgeons (RCS) rats (6–8 weeks old, male) were generously provided by the research group of Professor Guotong Xu. All animals were randomly assigned to the experimental group and the control group, with three animals in each group. All animals were housed in the Laboratory Animal Center of the Eye Research Institute, Shandong First Medical University. The usage, management, feeding, and immunological testing of experimental animals were strictly carried out in accordance with the National Implementing Rules for the Management of Medical Laboratory Animals. All animal management and animal experiments were conducted in strict accordance with the principles of management and use of experimental animals declared by ARVO and IACUC, and all experimental steps were reviewed and approved by the Laboratory Animal Ethics Committee of Shandong Eye Research Institute.

UVA-induced mouse model

A UVA LED light source (M365LP1, Thorlabs) with an emission peak of 365 nm light, 9 nm bandwidth (FWHM), and irradiance of 398 mW/cm^2 was focused to illuminate a 4-mm-diameter spot onto the mouse cornea. The energy was measured using a laser sensor (Model L49-150A, OphirPhotonics, Israel), and the time of UVA exposure was adjusted to deliver the appropriate fluence (20 min 57 s for 500 J/cm^2)[33]. The right eye was irradiated while the contralateral eye was covered with heat retention drapes (SpaceDrapes, Inc.) to serve as an untreated control. Mice were euthanized by cervical dislocation seven days after UVA irradiation.

Establishment of a corneal endothelial dysfunction model in rabbits

Rabbits were weighed, followed by an intramuscular injection of xylazine hydrochloride at a dosage of 0.1 ml/kg. Once the muscles were relaxed, the rabbits were anesthetized using an intravenous injection of 3.0% sodium pentobarbital at a dosage of 25 mg/kg, administered at the ear margin. The rabbits lost their eyelid and corneal reflexes, and experienced a decrease in muscle tension, and a deepening of respiration with a consistent frequency, signifying their transition into the anesthesia and surgical period. Prepare for the next step of liquid nitrogen condensation. A 6-mm diameter rounded metal rod was immersed in liquid nitrogen for 10 minutes to ensure it reached a fully cold state. Subsequently, a rabbit lid opener was utilized to lift the eyelid and dry the surface of the eye. The pre-cooled metal rod was then positioned at the center of the cornea for 30 s, after which it was removed and a waiting period of 1 minute was observed. This procedure was repeated to achieve the desired condensation effect[34]. Slit lamp photography (SL-D301, Topcon, Japan) and anterior segment OCT (XR, Optovue Inc., USA) were performed to measure the CCT, and corneal clarity grading scores before condensation, as well as on the 1, 3, 7, 10, and 14 days following the condensation procedure[35].

Immunofluorescence staining

Fresh corneal tissues were harvested and fixed at room temperature with 4% paraformaldehyde for 12 minutes. SD and RCS rats were euthanized by decapitation, and their eyes were promptly removed and fixed in 4% paraformaldehyde for preservation[36]. During preparation, the muscles and connective tissues were meticulously dissected under a microscope, followed by careful excision of the cornea, iris, and lens. The eye cup was then sectioned into four radial slices from the periphery towards the optic papilla. The retinal layer was carefully detached, ensuring the preservation of the RPE-Bruch's membrane-choriocapillaris complex (RBCC) and sclera. 0.1% Triton X-100 (T8200, Solarbio) was used to permeabilize the tissue for a duration of 10 minutes, followed by washing with PBS. Subsequently, the tissue was blocked with 10% donkey serum at room temperature for 30 minutes. Following another wash with PBS, antibodies ZO-1 (40-2200, Invitrogen), Tom20 (80501-1-12 R, Abcam), Hsp70 (10995-1-AP, Proteintech), and γ-H2AX (81299, Abcam) were applied dropwise and incubated overnight at 4 °C. Alexa Fluor 488 and Alexa Fluor 594 conjugated secondary antibodies (Invitrogen) were added and incubated at 37 °C for 1 h. The cell nucleus was stained with DAPI (C0065 Solarbio) before fluorescence staining. Images were captured using a confocal microscope (LSM 880, Zeiss, Germany). ZO-1 images were processed by Photoshop (Version 22.0.0), and data were extracted to calculate XV.

Alizarin red staining

Freshly obtained rabbit corneal tissues were carefully placed endothelial side up on a slide. 0.2% alizarin red solution was carefully applied to the endothelial surface of the rabbit cornea with a staining duration of 1.5 minutes. The cornea was gently rinsed 2 times with 0.9% saline until all the red hue in the washing solution was gone. The cornea was then covered with a coverslip and examined under a microscope (DM4B, Leica, Germany). Images were obtained using a white light background and a magnification of 10×, then cropped to 608 × 892 pixels for further image recognition analysis. The acquired images were processed by Image J (Version 1.51j8), and the data were extracted to calculate the XV.

Statistical analysis

All quantitative variables were tested for normality using the Shapiro-Wilk test. Variables with normal distribution were presented as mean ± standard deviation $\bar{x} \pm sd$ and compared using one-way ANOVA with LSD for post-hoc tests. Non-normally distributed variables were expressed as median (M[P25, P75]) and compared using the Kruskal-Wallis H test, with multiple comparisons performed by the Dunnett method. Categorical variables were summarized as percentages and compared using the chi-square test or Fisher's exact test, as appropriate. The intraclass correlation coefficient (ICC) was used to evaluate the consistency of the results of the new measures of CD and AVE with the gold standard measures. The diagnostic performance of the XV and the CV was evaluated using ROC analysis, with sensitivity, specificity, and AUC as assessment metrics. The diagnostic value of multiple parameters was compared using LDA. A global optimization strategy was applied to identify the best parameter combination, with 10-fold cross-validation to reduce overfitting, and performance was evaluated by accuracy, sensitivity, and specificity. Spearman's rank correlation was used to assess the association between single-cell XV percentage and corneal thickness. Concordance between the two functional grading methods was evaluated using confusion matrix analysis on the clinical validation set. All statistical analyses were performed using R (version 4.3.3), with $P < 0.05$ considered statistically significant. Statistical figures were generated using GraphPad Prism (version 9.0.0 (121)).

Data availability

The data supporting the main findings of this study are available in the main manuscript and the Supplementary Information. Due to institutional regulations and patient privacy restrictions imposed by participating hospitals, the raw datasets cannot be made publicly available. However, anonymized data are available for research purposes and can be requested from the corresponding authors upon reasonable request.

Code availability

The code used for dataset preparation, statistical modeling, and evaluation of the study findings is available in the GitHub repository at https://github.com/wang-xin-hang/Cell-code.

Received: 26 December 2024; Accepted: 2 December 2025;
Published online: 22 December 2025

References

1. Jeang, L. J., Margo, C. E. & Espana, E. M. Diseases of the corneal endothelium. *Exp. Eye Res.* **205**, 108495 (2021).
2. Price, M. O., Mehta, J. S., Jurkunas, U. V. & Price, F. W. Jr. Corneal endothelial dysfunction: Evolving understanding and treatment options. *Prog. Retin. Eye Res*. **82**, 100904 (2021).
3. Armitage, W. J., Dick, A. D. & Bourne, W. M. Predicting endothelial cell loss and long-term corneal graft survival. *Invest. Ophthalmol. Vis. Sci.* **44**, 3326–3331 (2003).
4. Klyce, S. D. 12. Endothelial pump and barrier function. *Exp. Eye Res.* **198**, 108068 (2020).
5. Yuan, S. & Fan, G. Stem cell-based therapy of corneal epithelial and endothelial diseases. *Regen. Med.* **10**, 495–504 (2015).
6. Anna-Katharina, S. et al. Bringing together the eye banking community throughout Europe and beyond – promoting eye donation in Africa. *BMJ Open Ophthalmol.* **8**, P24–A114 (2023).
7. McCarey, B. E., Edelhauser, H. F. & Lynn, M. J. Review of corneal endothelial specular microscopy for FDA clinical trials of refractive procedures, surgical devices, and new intraocular drugs and solutions. *Cornea* **27**, 1–16 (2008).
8. Konan Inc. KONAN MEDICAL [CellCheck Overview Video]. https://konanmedical.com/cellchek (2020).
9. Ting, D. S. W. et al. Development and validation of a deep learning system for diabetic retinopathy and related eye diseases using retinal images from multiethnic populations with diabetes. *JAMA* **318**, 2211–2223 (2017).
10. Milea, D. et al. Artificial intelligence to detect Papilledema from Ocular Fundus Photographs. *N. Engl. J. Med.* **382**, 1687–1695 (2020).
11. Karmakar, R., Nooshabadi, S. & Eghrari, A. An automatic approach for cell detection and segmentation of corneal endothelium in specular microscope. *Graefes Arch. Clin. Exp. Ophthalmol.* **260**, 1215–1224 (2022).
12. Daniel, M. C. et al. Automated segmentation of the corneal endothelium in a large set of 'real-world' specular microscopy images using the U-Net architecture. *Sci. Rep.* **9**, 4752 (2019).
13. Karmakar, R., Nooshabadi, S. V. & Eghrari, A. O. Mobile-CellNet: Automatic Segmentation of Corneal Endothelium Using an Efficient Hybrid Deep Learning Model. *Cornea* **42**, 456–463 (2023).
14. Writing Committee for the Cornea Donor Study Research Group, et al. Factors associated with corneal graft survival in the cornea donor study. *JAMA Ophthalmol*. **133**, 246–254 (2015).
15. Terry, M. A. et al. Donor, recipient, and operative factors associated with graft success in the cornea preservation time study. *Ophthalmology* **125**, 1700–1709 (2018).
16. Wilhelm, T. I. et al. Ten-year outcomes after DMEK, DSAEK, and PK: insights on graft survival, endothelial cell density loss, rejection and visual acuity. *Sci. Rep.* **15**, 1249 (2025).
17. Tsai, M. C. & Daniels, J. T. The impact of biomechanics on corneal endothelium tissue engineering. *Exp. Eye Res.* **209**, 108690 (2021).
18. Brookes, N. H. Riding the cell jamming boundary: Geometry, topology, and phase of human corneal endothelium. *Exp. Eye Res.* **172**, 171–180 (2018).
19. Müller, A., Doughty, M. J. & Wright, L. Reassessment of the corneal endothelial cell organisation in children. *Br. J. Ophthalmol.* **84**, 692–696 (2000).

20. Rao, G. N., Lohman, L. E. & Aquavella, J. V. Cell size-shape relationships in corneal endothelium. *Invest. Ophthalmol. Vis. Sci.* **22**, 271–274 (1982).
21. Ong Tone, S. et al. Fuchs endothelial corneal dystrophy: The vicious cycle of Fuchs pathogenesis. *Prog. Retin Eye Res.* **80**, 100863 (2021).
22. Vigueras-Guillén, J. P. et al. DenseUNets with feedback non-local attention for the segmentation of specular microscopy images of the corneal endothelium with guttae. *Sci. Rep.* **12**, 14035 (2022).
23. Chen, H. & Murphy, R. F. Evaluation of cell segmentation methods without reference segmentations. *Mol. Biol. Cell.* **34**, ar50 (2023).
24. Sami, A. S. & Rahim, M. S. M. Trainable watershed-based model for cornea endothelial cell segmentation. *J. Intell. Syst.* **31**, 370–392 (2022).
25. Xie, L. X. Further Studies on the Functional Decompensation of Corneal Endothelial Cells. *Zhonghua Yan Ke Za Zhi.* **25**, 141–143 (1989).
26. Kinoshita, S. et al. Grading for corneal endothelial damage. *Nippon Ganka Gakkai Zasshi.* **118**, 81–83 (2014).
27. Li, D. et al. Assessment of Corneal Endothelial Barrier Function Based on "Y-Junctions": A Finite Element Analysis. *Invest Ophthalmol. Vis. Sci.* **66**, 33 (2025).
28. Doughty, M. J. Non-contact specular microscopy with Topcon instruments to assess central corneal thickness of healthy human eyes - A 20 year review. *Cont. Lens Anterior Eye.* **44**, 101385 (2021).
29. Takahashi, H. Corneal Endothelium and Phacoemulsification. *Cornea* **35**, S3–S7 (2016). Suppl 1.
30. Moon, C. E. et al. Integrated Analysis of Transcriptome and Proteome of the Human Cornea and Aqueous Humor Reveal Novel Biomarkers for Corneal Endothelial Cell Dysfunction. *Int J. Mol. Sci.* **24**, 15354 (2023).
31. Kitazawa, K. et al. The biologic character of donor corneal endothelial cells influences endothelial cell density post successful corneal transplantation. *Ophthalmol. Sci.* **3**, 100239 (2022).
32. Huang, J. et al. Comparison of the center and flex-center methods of corneal endothelial cell analysis in the presence of Guttae. *Cornea* **36**, 1514–1520 (2017).
33. Liu, C. et al. Ultraviolet A light induces DNA damage and estrogen-DNA adducts in Fuchs endothelial corneal dystrophy causing females to be more affected. *Proc. Natl. Acad. Sci. Usa.* **117**, 573–583 (2020).
34. Ma, D. J. et al. Role of NADPH Oxidase 4 in Corneal Endothelial Cells Is Mediated by Endoplasmic Reticulum Stress and Autophagy. *Antioxidants* **12**, 1228 (2023).
35. Bandeira, F., Goh, T. W., Setiawan, M., Yam, G. H. & Mehta, J. S. Cellular therapy of corneal epithelial defect by adipose mesenchymal stem cell-derived epithelial progenitors. *Stem Cell Res Ther.* **11**, 14 (2020).
36. Zhang, J. et al. A modified histoimmunochemistry-assisted method for in situ RPE evaluation. *Front Biosci. (Elite Ed.).* **4**, 1571–1581 (2012).

Acknowledgements

This study received funding from the National Science Fund for Distinguished Young Scholars (82325014), the Shandong Provincial Key Research and Development Program (2021ZDSYS14), the Joint Innovation Team for Clinical & Basic Research (202405), the Taishan Scholar Program (tstp20221163 and tsqn 202312370), and the National Natural Science Foundation of China (82571185). We thank Dr. Hanruo Liu for the valuable contributions to the manuscript revision and constructive suggestions.

Author contributions

All authors read and approved the final version of the manuscript. L.X., Q.Z., and Z.L. designed the study and supervised the project. D.L., W.S., S.W. Collection data. D.L., H.D., X.H., and X.L. performed the experiments. Z.L., D.L., Q.Q. analyzed the data and developed the methodology. X.W., K.D. contributed to data visualization. D.L., Z.L. wrote the manuscript.

Competing interests

Chinese invention patentApplication Number: 2024110122687 Applicant: Shandong Eye Institute Affiliated of Shandong First Medical University (Shandong Eye Institute, Qingdao Eye Hospital Affiliated of Shandong First Medical University). Inventors: Lixin Xie, Zongyi Li, Dongfang Li, Ping Lin, Qingjun Zhou, Xinhang Wang. Title of the Invention: A Method for Evaluating the Function of Individual Corneal Endothelial Cells Based on Cell Morphology Application. Status: Substantive Examination Phase Patent Manuscript: Uploaded to the Related files.

Additional information

Supplementary information The online version contains supplementary material available at https://doi.org/10.1038/s41746-025-02239-0.

Correspondence and requests for materials should be addressed to Qingjun Zhou or Lixin Xie.